Progress In Electromagnetics Research, PIER 78, 103–127, 2008

MUTUAL COUPLING OF PRINTED ELEMENTS ON A CYLINDRICALLY LAYERED STRUCTURE USING CLOSED-FORM GREEN'S FUNCTIONS

R. C. Acar

Aselsan Electronics Industries Inc. H.C. A.E.D.T.M.
ODTU Teknokent Yerleşkesi SATGEB-1 Alanı 06531, Ankara, Turkey

G. Dural

Department of Electrical and Electronics Engineering
Middle East Technical University
06531, Ankara, Turkey

Abstract—A hybrid method to calculate mutual coupling of electric or magnetic current elements on a cylindrically layered structure using closed-form Green's functions is presented. When $\rho = \rho'$ and ϕ is not very close to ϕ', closed-form Green's functions are employed in the calculation of MoM matrix entries. When both $\rho = \rho'$ and $\phi = \phi'$, series representation of the spectral domain Green's functions do not converge, therefore closed-form Green's functions can not be employed. In that case MoM matrix entries are evaluated using the proposed hybrid method. The technique is applied to both printed dipoles and slots placed on a layered cylindrical structures. The computational efficiency of the analysis of mutual coupling of printed elements on cylindrically layered geometries is increased with the use of proposed hybrid method which employs closed-form Green's functions.

1. INTRODUCTION

The importance of cylindrically layered structures has led to the investigation of the scattering from infinite conducting, dielectric or dielectric-coated conducting cylinders and the radiation from patches, microstrip lines on cylindrical structures and cylindrical-rectangular, wraparound microstrip antennas [1–20]. In this paper, a hybrid method which combines the use of closed-form Green's functions with the

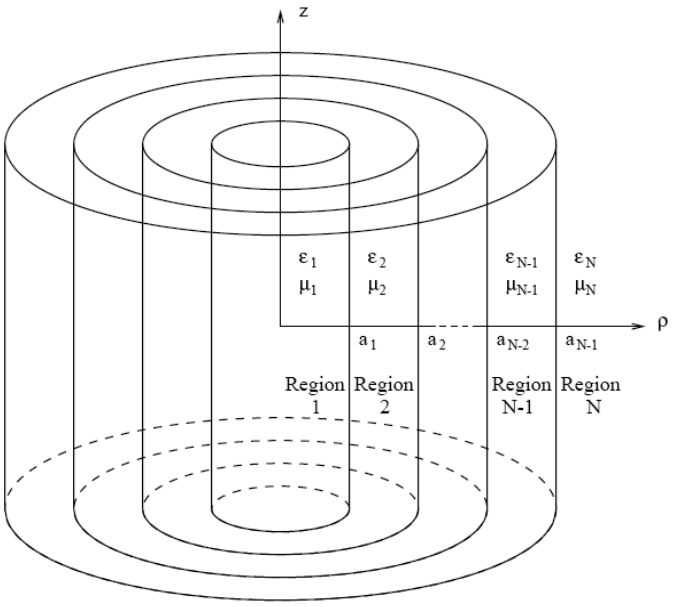

Figure 1. General cylindrically multilayered medium.

spectral domain analysis, is utilized to calculate the mutual coupling of printed elements on cylindrically stratified structures.

For the rigorous analysis of printed geometries in multilayer media, geometries, numerical algorithms based on the Method of Moments (MoM) are widely favored over other rigorous techniques, such as finite elements (FEM) and finite difference time domain methods (FDTD). The Method of Moments (MoM) is the most frequently used numerical technique to solve the problems of microstrip geometries mounted on multilayer structures. In this method, the integral equation is transformed into a matrix equation by approximating the unknown function in terms of known basis functions, then using testing functions the boundary conditions are applied to minimize the weighted error due to this approximation. When MoM is applied in the spatial domain, the numerical computation of MoM matrix entries is very time consuming. The reason for that is a difficulty with the numerical evaluation of the Sommerfeld integrals, which is mainly due to the oscillatory nature of the Sommerfeld integrals, and the slow-decaying nature of the spectral-domain Green's functions. Closed-form Green's functions can be used to improve numerical efficiency for the evaluation of MoM integral. For a general cylindrically layered medium shown in Fig. 1, closed-form Green's functions are

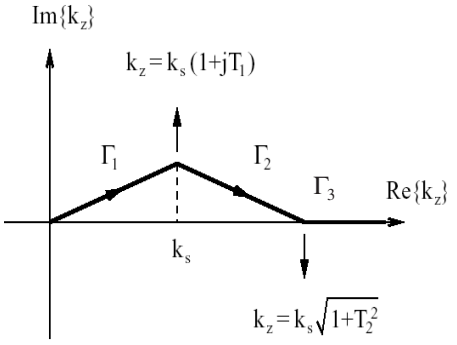

Figure 2. Deformed path.

obtained by approximating the spectral domain Green's function in terms of complex exponential functions in three consecutive steps on a deformed integration path shown in Fig. 2 and then transforming these exponential functions into the spatial domain analytically [21]. This technique eliminates the requirement of the time consuming transformation by the numerical integration of the inverse Fourier integral along the real axis on the complex k_z plane where the surface wave poles and the branch-point singularities are encountered. Therefore, spatial domain Green's functions are obtained in closed forms rather than numerically evaluating Sommerfeld integral which improves the numerical efficiency in the computation of the spatial domain Green's functions. Hence, analysis of different problems such as radiation from microstrips, patches and slots mounted on cylindrical surfaces, and scattering from dielectric shells and cylinders can be numerically improved, considerably.

In a previously reported work [21], closed-form Green's function components for ϕ and z oriented sources were presented where series representations of these Green's functions were convergent in the spectral domain when $\vec{\rho} \neq \vec{\rho}'$. In addition, in [22] a procedure was proposed to ensure convergence at $\rho = \rho'$ but still convergence problem exists when $\phi = \phi'$, i.e., $\vec{\rho} = \vec{\rho}'$. In this paper, the work presented in [21] and [22] is extended to a more general form, by adding the components which were not provided in [21] and using a similar procedure outlined in [22] to make these Green's functions convergent at $\rho = \rho'$ so that they can be used in the analysis of printed structures using MoM with the aid of the method discussed in Section 3.

In this paper, the mutual coupling between two strips and between two slots placed on a cylindrically layered medium using MoM incorporation with the closed-form Green's functions is discussed. For

the calculation of the MoM matrix entries, a hybrid method is used, depending on whether ϕ is close to ϕ' or not. When $\rho = \rho'$, if ϕ is not close to ϕ' the closed-form Green's functions are employed. When ϕ is close to ϕ', since the spectral-domain Green's functions do not converge, $(\phi - \phi')$ difference term is handled in the convolutional integral in the spectral-domain in the calculation of MoM matrix elements. The technique is applied to both printed dipoles and slots placed on a layered cylindrical structure. The computational efficiency of the anaysis of mutual coupling of printed elements on cylindrically layered structures is increased with the use of proposed hybrid method due to use of closed-form Green's functions.

2. GREEN'S FUNCTION FORMULATION

A cylindrically layered geometry is shown in Fig. 1. An electric or magnetic source of z or ϕ orientation is embeded in region j and the observation point may be located in any layer, denoted by region i. Layers may vary in their electric or magnetic properties (ε, μ) as well as the thickness. The method can also be applied to lossy dielectric material. First the axial components of the spectral domain electric and magnetic fields are derived for the source layer, then these field components are transferred into the observation layer using a recursive algorithm [21].

Spectral domain Green's functions can be transformed into spatial domain by evaluating the Sommerfeld integral,

$$G^{E,H}(z - z') = \frac{1}{2\pi} \int_{-\infty}^{\infty} e^{-jk_z(z-z')} \tilde{G}^{E,H}(k_z) dk_z \tag{1}$$

where $G^{E,H}$ denotes spatial domain Green's function. Since the numerical evaluation of (1) has difficulties and is very time consuming, to improve computational efficiency the deformed path [21] given in Fig. 2. is used as the path of integration in (1). The spectral domain Green's functions are approximated in terms of complex exponential functions in three consecutive steps and then these exponential functions are transformed into the spatial domain, analytically.

The z and ϕ oriented components of spatial domain closed-form Green's functions for an electric and a magnetic dipole pointing in z and ϕ direction were given in [21]. The remaining spatial domain closed-form Green's function components which are not given in [21] are also obtained and the complete set of spectral-domain Green's functions is presented in the Appendix for the sake of completeness. Additionally, the surface wave contribution in cylindrically stratified

media is investigated. In that study, the effect of the surface wave poles and the selection of the deformed path parameters are studied. When a proper deformed path is used in the evaluation of spatial-domain Green's functions, it is observed that removing the surface wave contributions from spectral-domain Green's functions does not provide an extra benefit [23].

The spatial domain Green's functions given by [21] can only be evaluated when ρ is not equal to ρ'. However, when MoM is applied in the spatial domain, the spatial domain Green's functions at $\rho = \rho'$ is needed. To make the series representations of these Green's functions convergent in spectral domain when $\rho = \rho'$ a similar procedure reported in [22] is employed.

To demonstrate the procedure, the spectral domain Green's function $\tilde{G}^E_{zz}$ is considered in this paper, where $\tilde{G}^E_{zz}$ has a summation term $S_1 = \sum_{n=-\infty}^{\infty} f_{11} e^{jn(\phi-\phi')}$ that has a convergence problem when $\rho = \rho'$, therefore infinite number of terms are needed to obtain a convergent result. It is realized that the quasistatic components of f_{11} are slowly convergent, on the other hand the inverse Fourier transform of the quasistatic components has a closed form. After the quasistatic components are completely extracted from the Green's functions in spectral domain, the remaining parts have good convergence behaviours which can be used to speed up the calculation of the inverse Fourier transform. Then the quasistatic components are transformed into spatial domain analytically and their contributions are added in closed form [22].

The summation term, S_1 can be expressed as

$$\begin{aligned} S_1 &= \sum_{n=-\infty}^{\infty} \frac{f_{11}}{\left(H_n^{(2)}(k_{\rho_i}\rho)J_n(k_{\rho_i}\rho')\right)} \left(H_n^{(2)}(k_{\rho_i}\rho)J_n(k_{\rho_i}\rho')\right) e^{jn(\phi-\phi')} \\ &= \sum_{n=-\infty}^{\infty} C_1 \left(H_n^{(2)}(k_{\rho_i}\rho)J_n(k_{\rho_i}\rho')\right) e^{jn(\phi-\phi')} \end{aligned} \tag{2}$$

where $J_n()$ and $H_n^{(2)}()$ are nth order first-kind Bessel function and nth order second-kind Hankel function, respectively.

The coefficient C_1 depends on n and k_z; if k_z is fixed then C_1 only depends on n. With increasing n, C_1 has an asymptotic value denoted as C_1^*. C_1^* is independent of n, but depends on k_z.

$$\lim_{n\to\infty} C_1(n, k_z) \cong C_1^*(k_z)$$

While moving along the Sommerfeld integration path on Γ_3 path, C_1^* is found to be almost a constant that is denoted as C_1^{**} ; hence C_1^{**} is

independent of n and k_z.

$$\lim_{k_z \to \infty} C_1^*(k_z) \cong C_1^{**}$$

As a summary, the complete procedure can be outlined as follows:

- The spectral domain Green's functions are evaluated uniformly along the deformed path given in Fig. 2 [21].
- The asymptotic terms C_1^* and C_1^{**} are subtracted to make the remains of the Green's function vanishing on path Γ_3 and are transformed into those in spatial domain in closed form [22].
- The resultant Green's functions are sampled uniformly along two deformed paths Γ_1 and Γ_2 and approximated in terms of N_1 and N_2 complex exponentials of k_z by using the Generalized Pencil of Function (GPOF) method [24].
- Transforming the approximated Green's functions into the spatial domain turns out to be a simple contour integral of exponentials which have closed forms.

3. MUTUAL COUPLING ANALYSIS

Main contribution of this paper is to employ closed-form Green's functions to evaluate the MoM matrix entries in order to increase the computational efficiency in the analysis of cylindrically multilayer geometries. Since when $\rho = \rho'$ and $\phi = \phi'$ numerical difficulties exist in the evaluation of closed-form Green's functions, a hybrid method is used. The hybrid method employs the closed-form Green's functions in the spatial domain whenever ϕ is not close to ϕ', otherwise $(\phi - \phi')$ difference term is handled with the convolutional integral in the spectral domain. Using closed-form Green's functions in the evaluation of MoM matrix entries avoids the requirement of the tedious and time consuming numerical integration of the Sommerfeld integral where the surface wave poles and the branch point singularities are encountered. Since the closed-form expressions of the Green's functions derived for a specific point remain to be valid when the z coordinate of this point is altered, the need for recomputing the Green's functions for the points with varying z coordinates is eliminated. Hence, the proposed hybrid method saves great amount of computational time in the calculation of MoM matrix elements.

In this section, the analysis of mutual coupling between two narrow strips and between two narrow slots placed on a cylindrically layered medium is presented. Mutual impedance and mutual coupling coefficient formulations are also provided for both strip and slot

examples to demonstrate the use of both electric and magnetic type Green's functions in cylindrically layered media.

3.1. Mutual Coupling between Two Strips

A cylindrical 3-layer medium with two narrow strips placed on $\rho = a_1$ is given in Fig. 3.

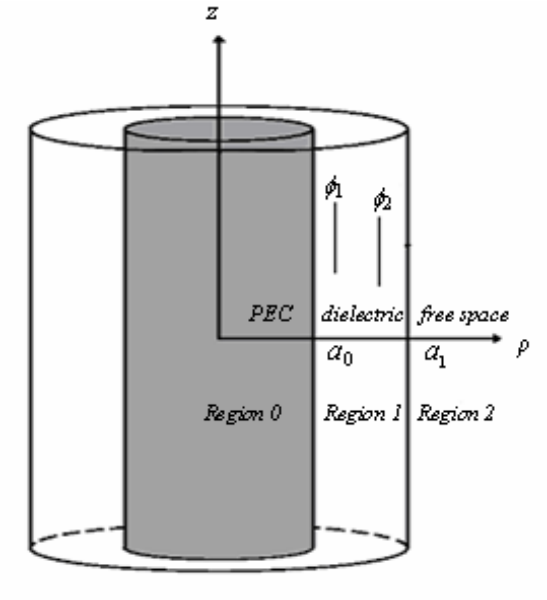

Figure 3. A 3-layer structure with Region 0: PEC, Region 1: $\varepsilon_{r_1} = 2.3$, $\mu_{r_1} = 1$, Region 2: free space, $a_0 = 20\,\text{mm}$, $a_1 = 21\,\text{mm}$, $f = 4.7\,\text{GHz}$.

For the spatial domain MoM formulation, the typical matrix equation can be written in the following form

$$\begin{bmatrix} \left\langle \overline{J}_{m1}, \overline{G}^E * \overline{J}_{n1} \right\rangle & \left\langle \overline{J}_{m1}, \overline{G}^E * \overline{J}_{n2} \right\rangle \\ \left\langle \overline{J}_{m2}, \overline{G}^E * \overline{J}_{n1} \right\rangle & \left\langle \overline{J}_{m2}, \overline{G}^E * \overline{J}_{n2} \right\rangle \end{bmatrix} \begin{bmatrix} a_{n1} \\ a_{n2} \end{bmatrix} = \begin{bmatrix} -\left\langle \overline{J}_{m1}, \overline{G}^E * \overline{J}^i \right\rangle \\ -\left\langle \overline{J}_{m2}, \overline{G}^E * \overline{J}^i \right\rangle \end{bmatrix} \tag{3}$$

where $m_i, n_i = 1, \ldots, N,\ i = 1, 2$, $*$ denotes convolution, $\overline{J}^i$ is taken as a delta gap source, $\overline{J}_{m1}, \overline{J}_{n1}$ and $\overline{J}_{m2}, \overline{J}_{n2}$ are testing and basis functions of the first strip and the second strip, respectively.

The matrix entries in (3) can be written in the following form

$$Z_{mn} = \iint dz dl J_{mz}(z, l) \iint dz' dl' G^E_{zz}(z - z', l - l') J_{nz}(z', l') \tag{4}$$

where l and l' are the "arc length" variables which are given as $l = a_1\phi$ and $l' = a_1\phi'$.

Galerkin's procedure is employed in the mutual coupling analysis with the selection of testing function $\overline{J}_m$ and basis function $\overline{J}_n$ of each strip same. This choice results in a symmetric matrix, hence considerably reduces the computation time of Z_{mn}.

By changing of variables $u = z - z'$ and $v = l - l'$, (4) can be written as

$$Z_{mn} = \iint dzdl \iint dudv G^E_{zz}(u,v) J_{mz}(z,l) J_{nz}(z-u, l-v) \tag{5}$$

Putting the closed-form of G_{zz} [21] given in (6) into (5), (7) is obtained,

$$G^E_{zz}(u,v) = \frac{1}{2\pi} \int dk_z e^{-jk_z(z-z')} \sum_k G^k_{zz}(\rho = \rho', k_z) e^{jk(\phi-\phi')} \tag{6}$$

$$\begin{aligned} Z_{mn} \;=\; & \iint dzdl \iint dudv \left\{ \frac{1}{2\pi} \int dk_z e^{-jk_z(z-z')} \left(\sum_k G^k_{zz} e^{jk(\phi-\phi')} \right) \right\} \\ & \times J_{mz}(z,l) J_{nz}(z-u, l-v) \end{aligned} \tag{7}$$

Expressing the current density J_{mz} by a rooftop function, i.e., a Triangular function in z direction and a Pulse function in ϕ direction, i.e., $J_{mz} = T_{mz}(z) P_{mz}(l)$ and changing the order of integrals, (8) is obtained,

$$\begin{aligned} Z_{mn} \;=\; & \iint dudv \left\{ \frac{1}{2\pi} \int dk_z e^{-jk_z u} \left(\sum_k G^k_{zz} e^{jk(\phi-\phi')} \right) \right\} \\ & \times \int dl P_{m\phi}(l) P_{n\phi}(l-v) \int dz T_{mz}(z) T_{nz}(z-u) \end{aligned} \tag{8}$$

For the calculation of (8), a hybrid method is used, depending on whether ϕ is close to ϕ' or not. If ϕ is not close to ϕ' the closed-form Green's functions are employed. When ϕ is close to ϕ', since the spectral-domain Green's functions do not converge, $(\phi - \phi')$ difference term is handled with the convolutional integral in the spectral-domain in the calculation of MoM matrix element Z_{mn}.

To be more explanatory, the last integral in (8), which is a convolution integral, is evaluated analytically. For the rest of the calculation of the matrix entry Z_{mn}, a hybrid method is used:

- when ϕ is not close to ϕ', the 'dl' integration and the closed-form of G^F_{zz} are evaluated independently; MoM matrix elements are obtained in the spatial domain,

- when ϕ is close to ϕ', (9) is obtained from (8) and used for the calculation for the matrix entry Z_{mn} such as: first, Pulse functions are integrated giving an analytical result in terms of v, then the multiplication of this analytical term with e^{jkv} is used as an integrand in v integration, at the last step, the spectral domain k_z integral is calculated in closed-form.

$$Z_{mn} = \int du \left\{ \frac{1}{2\pi} \int dk_z e^{-jk_z u} \left\{ \sum_k G_{zz}^k \int dv e^{jkv} \left(\int dl P_{m\phi}(l) P_{n\phi}(l-v) \right) \right\} \right\} \times \left\{ \int dz T_{mz}(z) T_{nz}(z-u) \right\} \tag{9}$$

3.2. Mutual Coupling between Two Slots

A cylindrical 3-layer medium with two narrow slots placed on $\rho = a_1$ is given in Fig. 4. For this geometry, the slot is represented by an equivalent magnetic-current distribution $\overline{J}^m$ by using the equivalence principle. Therefore Green's functions due to magnetic current elements are employed.

Since the tangential electric field across the slot can be represented by the equivalent magnetic-current distribution

$$\overline{J}^m = \overline{E} \times \hat{n} = \overline{E} \times \hat{a}_\rho \tag{10}$$

The unit normal to the surface is denoted by $\hat{n}$ which is $\hat{a}_\rho$ for this problem.

The equivalent magnetic-current distributions inside and outside of PEC can be written as

$$\text{For } \rho > a_1, \qquad \overline{J}_{out}^m = \overline{E} \times \hat{a}_\rho = E_\phi \hat{a}_\phi \times \hat{a}_\rho = -E_\phi \hat{a}_z \tag{11}$$

$$\text{For } \rho < a_1, \qquad \overline{J}_{in}^m = \overline{E} \times (-\hat{a}_\rho) = E_\phi \hat{a}_\phi \times (-\hat{a}_\rho) = E_\phi \hat{a}_z \tag{12}$$

We shall use the boundary condition that the tangential magnetic field is continous across the aperture,

$$\overline{H}_z^{in} \left(\overline{J}_{in}^m \right) = \overline{H}_z^{out} \left(\overline{J}_{out}^m \right) + \overline{J}_s \delta(z-d) \quad \text{at } \rho = a_1 \tag{13}$$

where $\overline{J}_s$ is the known probe current density at $z = d$.

Knowing that $\overline{H}^{in} = \overline{G}^H * \overline{J}_{in}^m$ and $\overline{H}^{out} = \overline{G}^H * \overline{J}_{out}^m$, (13) can be written as

$$\left(\overline{G}_{zz_{in}}^H * \overline{J}_{z_{in}}^m \right) = \left(\overline{G}_{zz_{out}}^H * \overline{J}_{z_{out}}^m \right) + \overline{J}_s \delta(z-d) \quad \text{at } \rho = a_1. \tag{14}$$

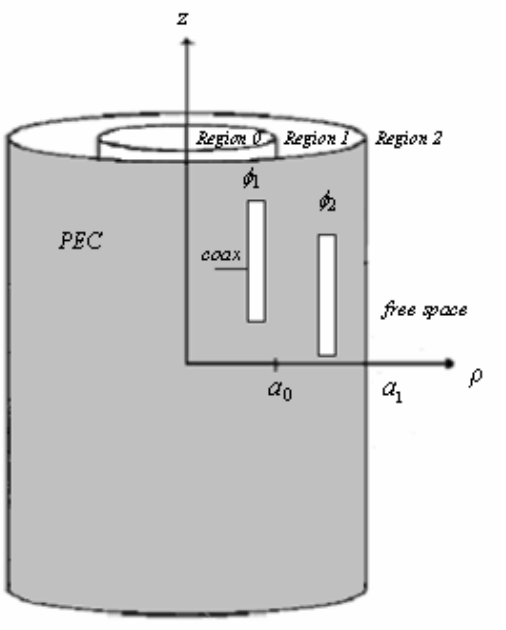

Figure 4. A 3-layer structure with Region 0: $\varepsilon_{r_0} = 2,\ \mu_{r_0} = 1$, Region 1: $\varepsilon_{r_1} = 5,\ \mu_{r_1} = 1$, Region 2: free space, $a_0 = 20\,\text{mm}$, $a_1 = 21\,\text{mm}$.

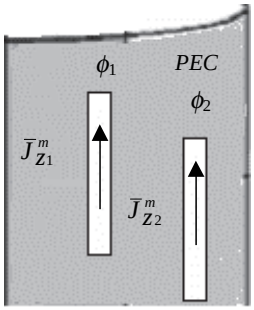

Figure 5. Equivalent magnetic current distributions on each slot.

Here, $\overline{G}^H_{zz}$ is the magnetic type Green's function in z direction due to z-oriented magnetic current source.

According to MoM, the total surface current density $\overline{J}^m_z$ can be expressed interms of N subsectional basis functions as

$$\overline{J}^m_{z_{in}} = -\overline{J}^m_{z_{out}} = \sum_{n1} a_{n1}\overline{J}_{n1} + \sum_{n2} a_{n2}\overline{J}_{n2} \tag{15}$$

where J_{n1} is basis function of the first slot, J_{n2} is the basis function of the second slot.

For the spatial domain MoM formulation, the typical matrix equation can be written as

$$\begin{bmatrix} \left\langle \overline{J}_{m1}, (\overline{G}^H_{zz_{in}} + \overline{G}^H_{zz_{out}}) * \overline{J}_{n1} \right\rangle & \left\langle \overline{J}_{m1}, (\overline{G}^H_{zz_{in}} + \overline{G}^H_{zz_{out}}) * \overline{J}_{n2} \right\rangle \\ \left\langle \overline{J}_{m2}, (\overline{G}^H_{zz_{in}} + \overline{G}^H_{zz_{out}}) * \overline{J}_{n1} \right\rangle & \left\langle \overline{J}_{m2}, (\overline{G}^H_{zz_{in}} + \overline{G}^H_{zz_{out}}) * \overline{J}_{n2} \right\rangle \end{bmatrix} \begin{bmatrix} a_{n1} \\ a_{n2} \end{bmatrix}$$
$$= \begin{bmatrix} \left\langle \overline{J}_{m1}, \overline{J}_s \delta(z-d) \right\rangle \\ \left\langle \overline{J}_{m2}, \overline{J}_s \delta(z-d) \right\rangle \end{bmatrix} \tag{16}$$

where $m_i, n_i = 1, \ldots, N,\ i = 1, 2,\ *$ denotes convolution, $\overline{J}_s$ is taken as a delta gap source, $\overline{J}_{m1}, \overline{J}_{n1}$ and $\overline{J}_{m2}, \overline{J}_{n2}$ are testing and basis functions of the first slot and the second slot, respectively.

The matrix entries in (16) can be written in the following form

$$Z_{mn} = \iint dz dl J_{mz}(z,l) \iint dz' d\phi' G^H_{zz}(z-z', l-l') J_{nz}(z', l') \tag{17}$$

In this application, the matrix entries Z_{mn} given in (17) are evaluated using the same procedure as applied in (4)–(9).

3.3. Mutual Impedance and Mutual Coupling Coefficient

The mutual impedance is given by [25]

$$Z_{21} = \iint\limits_{S_1} ds_1 \overline{J}_1(\overline{r}_1) \cdot \left(\iint\limits_{S_2} ds_2 \overline{G}(\overline{r}_1, \overline{r}_2) \overline{J}_2(\overline{r}_2) \right) \tag{18}$$

The coupling coefficient matrix $\overline{S}$ can be defined as [26],

$$\overline{S} = \begin{bmatrix} S_{11} & S_{12} \\ S_{21} & S_{22} \end{bmatrix} = \left(\overline{Z} - \overline{Z}_0 \right) \left(\overline{Z} + \overline{Z}_0 \right)^{-1} \tag{19}$$

Hence it can be written as,

$$\overline{S} = \begin{bmatrix} S_{11} & S_{12} \\ S_{21} & S_{22} \end{bmatrix}$$
$$= \left(\begin{bmatrix} Z_{11} & Z_{12} \\ Z_{21} & Z_{22} \end{bmatrix} - \begin{bmatrix} Z_0 & 0 \\ 0 & Z_0 \end{bmatrix} \right) \left(\begin{bmatrix} Z_{11} & Z_{12} \\ Z_{21} & Z_{22} \end{bmatrix} + \begin{bmatrix} Z_0 & 0 \\ 0 & Z_0 \end{bmatrix} \right)^{-1} \tag{20}$$

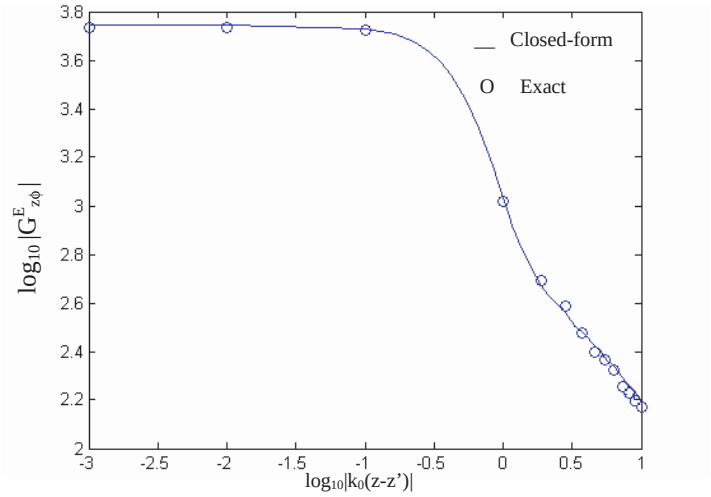

Figure 6. $\log_{10}|G^E_{z\phi}|$ for a magnetic dipole pointing in ϕ direction, for the geometry shown in Figure 3, $\rho = \rho' = 21\,\text{mm}$, $\phi - \phi' = 10^\circ$, $\varepsilon_{r_1} = 2.3$, $t_h = 1\,\text{mm}$, $f = 10\,\text{GHz}$.

Then, the mutual coupling coefficient S_{21} can be found as

$$S_{21} = \frac{2Z_{12}Z_0}{(Z_{11}+Z_0)(Z_{22}+Z_0) - Z_{12}Z_{21}} \tag{21}$$

where Z_0 is the characteristic impedance of the feeding coax which is assumed to be $50\,\Omega$.

4. NUMERICAL RESULTS AND DISCUSSIONS

A 3-layer structure in Fig. 3 with Region 0: PEC, Region 1: ε_{r_1}, $\mu_{r_1} = 1$, Region 2: free space, $a_1 = 20\,\text{mm}$, $a_2 = 21\,\text{mm}$, dielectric thickness $t_h = 1\,\text{mm}$, is presented to demonstrate the validity of the technique. $G^E_{z\phi}$ due to a magnetic dipole pointing in ϕ direction for $\phi - \phi' = 10^\circ$ and G^E_{zz} due to an electric dipole pointing in z direction for $\phi - \phi' = 15^\circ$ are calculated when $\rho = \rho' = 21\,\text{mm}$, which are given in Fig. 6 and Fig. 7, respectively. The exact (numerical integration of (1)) and our closed-form (approximate) Green's functions are plotted together and they are found to be in good agreement.

In Fig. 8 and Fig. 9 our results are compared with those given in [27] which is based on eigenfunction solution. The geometry given in Fig. 3 is used, each strip having $L = \lambda_0/2$ length and $0.002\,\lambda_0$ width, dielectric constant $\varepsilon_{r_1} = 2$.

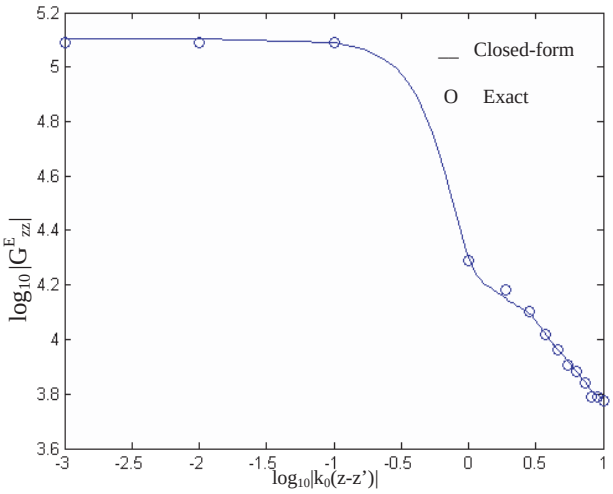

Figure 7. $\log_{10}|G^E_{zz}|$ for an electric dipole pointing in z direction, for the geometry shown in Figure 3, $\rho = \rho' = 21\,\text{mm}$, $\phi - \phi' = 15°$, $\varepsilon_{r_1} = 10$, $t_h = 1\,\text{mm}$, $f = 6.8\,\text{GHz}$.

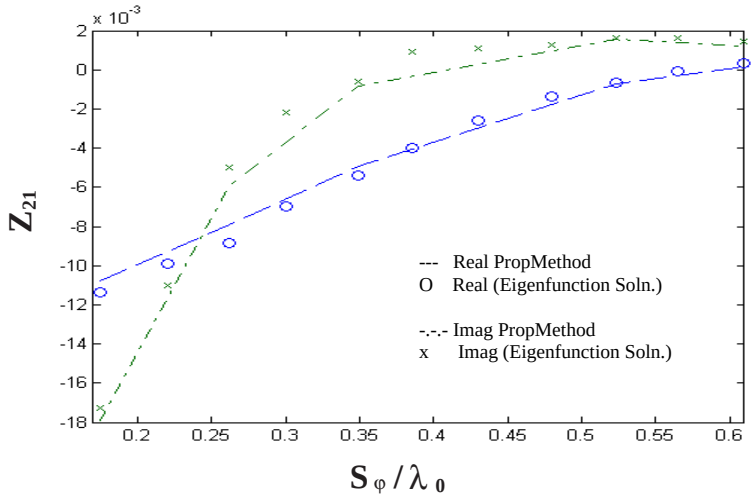

Figure 8. Real and Imaginary parts of the mutual impedance Z_{21} between two identical z-directed strips versus separation when $f = 4.7\,\text{GHz}$, $a_1 = 0.5\,\lambda_0$, $t_h = 0.02\,\lambda_0$, $L = \lambda_0/2$.

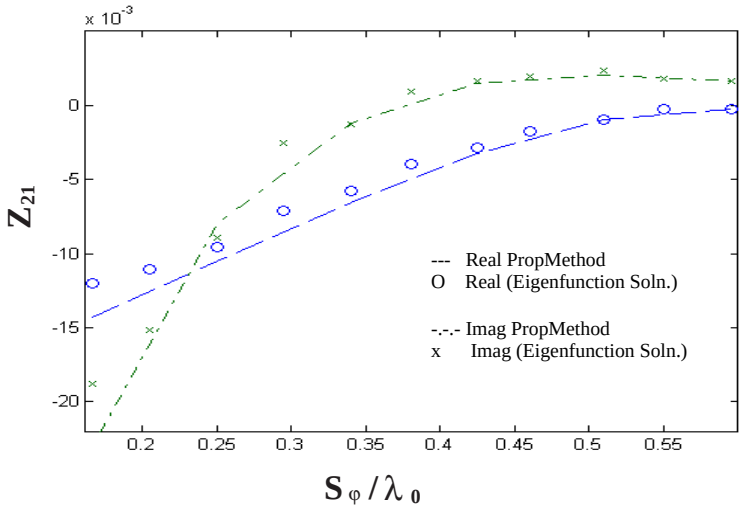

Figure 9. Real and Imaginary parts of the mutual impedance Z_{21} between two identical z-directed strips versus separation when $f = 2\,\text{GHz}$, $a_1 = 0.5\,\lambda_0$, $t_h = 0.02\,\lambda_0$, $L = \lambda_0/2$.

Fig. 8 shows mutual impedance Z_{21} between two identical z-directed strips versus S_φ when frequency f is 4.7 GHz and the outer cylinder radius 'a_1' is $0.5\,\lambda_0$, dielectric thickness 't_h' is $0.02\,\lambda_0$.

S_φ is the angular spacing between two z-directed strips with respect to free-space wavelength λ_0. Fig. 9 shows mutual impedance Z_{21} between two identical z-directed strips versus S_φ when frequency f is 2 GHz and the outer cylinder radius 'a_1' is $0.5\,\lambda_0$, dielectric thickness 't_h' is $0.02\,\lambda_0$.

It is clearly seen that the results for eigenfunction solution [27] and the proposed method in this paper are in good agreement with each other.

Mutual coupling between z-directed two narrow strips on a cylindrical 3-layer medium given in Fig. 3 is evaluated using the method discussed in the previous section. The excitation is done by a probe. Each strip has $L = \lambda_0/2$ length and $0.025\,\lambda_0$ width.

Fig. 10 and Fig. 11 show the mutual impedance Z_{21} and coupling coefficient S_{21} of two z-directed identical strips versus the angular spacing S_φ when $f = 4.7\,\text{GHz}$, $\varepsilon_{r_1} = 2.3$.

Mutual coupling between two z-directed narrow slots on a cylindrical 3-layer medium given in Fig. 4 is evaluated using the method discussed in the previous section. The geometry in Fig. 12 is used for

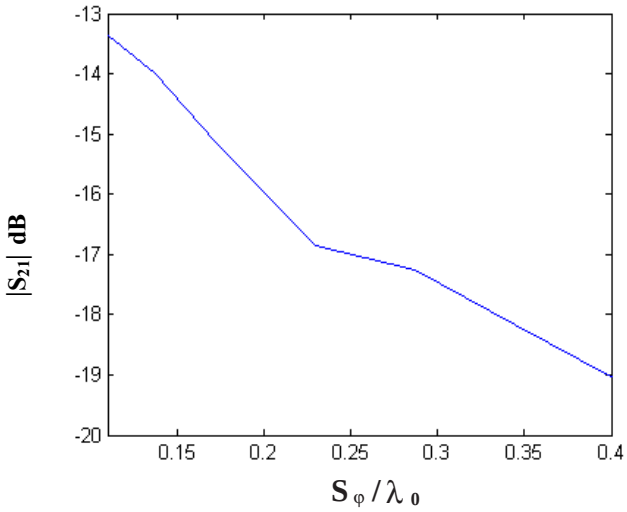

Figure 10. Mutual impedance Z_{21} for H-plane coupling case of two z-directed strips at $f = 4.7\,\text{GHz}$, $a_0 = 20\,\text{mm}$, $a_1 = 21\,\text{mm}$, $\varepsilon_{r_1} = 2.3$, $L = \lambda_0/2$.

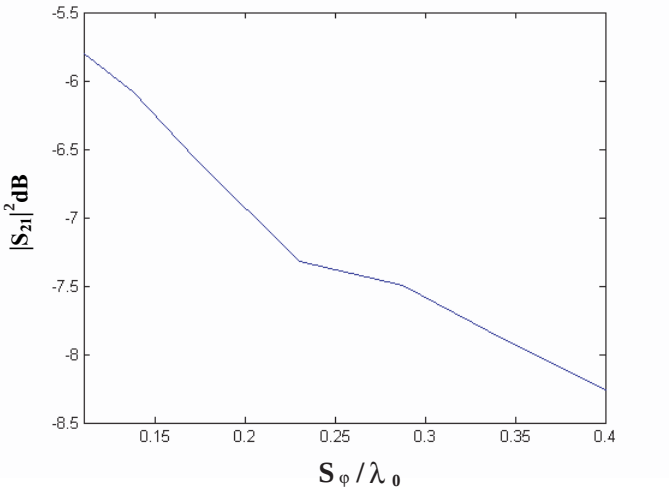

Figure 11. Mutual coupling coefficient S_{21} for H-plane coupling case of two z-directed strips at $f = 4.7\,\text{GHz}$, $a_0 = 20\,\text{mm}$, $a_1 = 21\,\text{mm}$, $\varepsilon_{r_1} = 2.3$, $L = \lambda_0/2$.

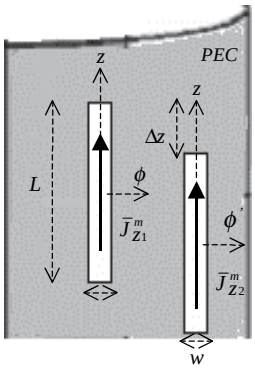

Figure 12. Geometry used for mutual coupling between two z-directed narrow slots.

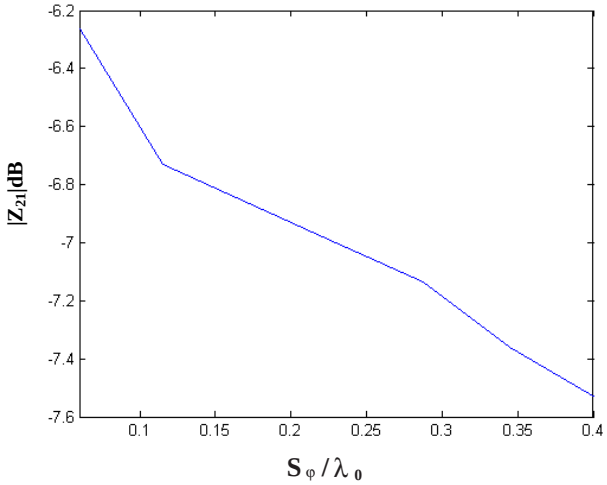

Figure 13. Mutual impedance Z_{21} for H-plane coupling case of two z-directed narrow slots at $f = 2\,\text{GHz}$, $a_0 = 20\,\text{mm}$, $a_1 = 21\,\text{mm}$, $\Delta z = 0$, $\varepsilon_{r_0} = 2$, $\varepsilon_{r_1} = 5$, $L = \lambda_0/2$.

the mutual coupling evaluation. The excitation is done by a coax by connecting the inner conductor of coax to the slot. Each slot has length as $L = \lambda_0/2$ and width as $w = 0.04\,\lambda_0$.

Fig. 13 and Fig. 14 show the mutual impedance Z_{21} of two z-directed narrow slots versus the angular spacing S_φ for $\Delta z = 0$ (the slots are parallel in z direction) and $\Delta z = \lambda_0/4$ values when $f = 2\,\text{GHz}$, $\varepsilon_{r_0} = 2$ and $\varepsilon_{r_1} = 5$.

Fig. 15 and Fig. 16 show the mutual coupling coefficient S_{21} of two

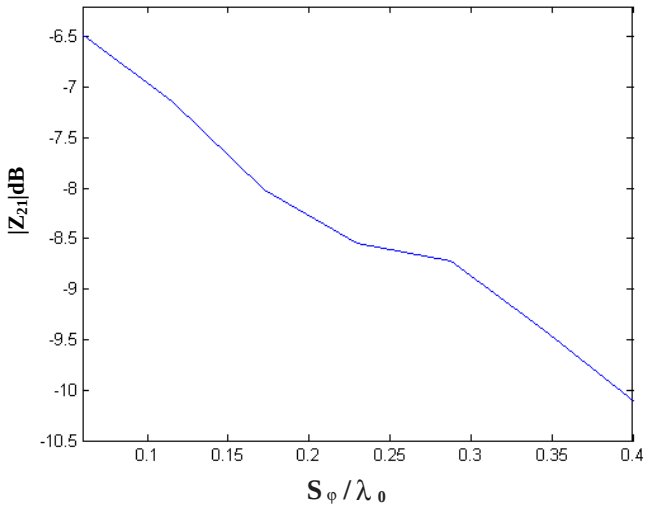

Figure 14. Mutual impedance Z_{21} for H-plane coupling case of two z-directed narrow slots at $f = 2\,\text{GHz}$, $a_0 = 20\,\text{mm}$, $a_1 = 21\,\text{mm}$, $\Delta z = \lambda_0/4$, $\varepsilon_{r_0} = 2$, $\varepsilon_{r_1} = 5$, $L = \lambda_0/2$.

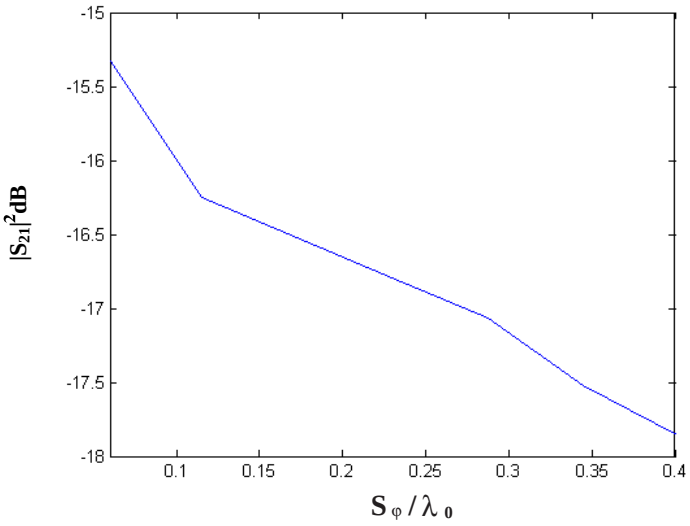

Figure 15. Mutual coupling coefficient S_{21} for H-plane coupling case of two z-directed narrow slots at $f = 2\,\text{GHz}$, $a_0 = 20\,\text{mm}$, $a_1 = 21\,\text{mm}$, $\Delta z = 0$, $\varepsilon_{r_0} = 2$, $\varepsilon_{r1} = 5$, $L = \lambda_0/2$.

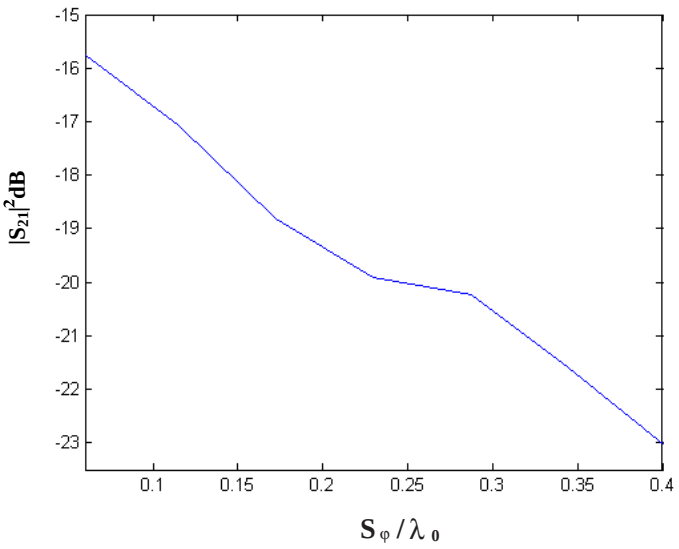

Figure 16. Mutual coupling coefficient S_{21} for H-plane coupling case of two z-directed narrow slots at $f = 2\,\text{GHz}$, $a_0 = 20\,\text{mm}$, $a_1 = 21\,\text{mm}$, $\Delta z = \lambda_0/4,\ \varepsilon_{r_0} = 2,\ \varepsilon_{r_1} = 5,\ L = \lambda_0/2$.

z-directed narrow slots versus the angular spacing S_φ for $\Delta z = 0$ (the slots are parallel in z direction) and $\Delta z = \lambda_0/4$ values when $f = 2\,\text{GHz}$, $\varepsilon_{r_0} = 2$ and $\varepsilon_{r_1} = 5$.

5. CONCLUSIONS

A hybrid method to calculate mutual coupling of electric or magnetic current elements on a cylindrically layered structure using MoM is presented. For the calculation of the MoM matrix entries, when $\rho = \rho'$, if ϕ is not close to ϕ', the closed-form Green's functions are employed. When ϕ is close to ϕ', since the spectral-domain Green's functions do not converge, MoM matrix elements are calculated in the spectral domain. The technique is applied to both microstriplines and slots placed on a layered cylindrical structure. The computational efficiency of the anaysis of mutual coupling of printed elements on a cylindrically layered structure is increased with the use of proposed hybrid method due to use of closed-form Green's functions.

Beside the presented geometries used in the analysis, multilayer coupling geometries such as slot-coupled microstrip patch antennas and slot antenna with microstrip feeding can also be analyzed.

APPENDIX A. SPECTRAL-DOMAIN GREEN'S FUNCTIONS

For the sake of completeness, complete-set of spectral-domain Green's functions are given as a reference. Among the spectral-domain Green's functions listed below, (A1)–(A4), (A7)–(A10), (A19)–(A22), (A25)–(A28) are given in [21]. The remaining spectral-domain Green's functions (A11)–(A18), (A23), (A24), (A29)–(A33), (A36) are given in [28] as corrections.

z-oriented electric dipole:

$$\tilde{G}_{zz}^{E_n} = \frac{k_{\rho_j}^2}{\varepsilon_j} f_{11} \tag{A1}$$

$$\tilde{G}_{zz}^{H_n} = \frac{k_{\rho_j}^2}{\varepsilon_j} f_{21} \tag{A2}$$

$$\tilde{G}_{\phi z}^{E_n} = \frac{k_{\rho_j}^2}{\varepsilon_j} \left(\frac{nk_z}{k_{\rho_i}^2 \rho} f_{11} + \frac{j\omega\mu_i}{k_{\rho_i}^2} \frac{\partial f_{21}}{\partial \rho} \right) \tag{A3}$$

$$\tilde{G}_{\phi z}^{H_n} = \frac{k_{\rho_j}^2}{\varepsilon_j} \left(-\frac{j\omega\varepsilon_i}{k_{\rho_i}^2} \frac{\partial f_{11}}{\partial \rho} + \frac{nk_z}{k_{\rho_i}^2 \rho} f_{21} \right) \tag{A4}$$

$$\tilde{G}_{\rho z}^{E_n} = \frac{k_{\rho_j}^2}{\varepsilon_j} \left(-\frac{jk_z}{k_{\rho_i}^2} \frac{\partial f_{11}}{\partial \rho} + \frac{\omega\mu_i n}{k_{\rho_i}^2 \rho} f_{21} \right) \tag{A5}$$

$$\tilde{G}_{\rho z}^{H_n} = \frac{k_{\rho_j}^2}{\varepsilon_j} \left(-\frac{\omega\varepsilon_i n}{k_{\rho_i}^2} \frac{f_{11}}{\rho} - j \frac{k_z}{k_{\rho_i}^2} \frac{\partial f_{21}}{\partial \rho} \right) \tag{A6}$$

ϕ-oriented electric dipole:

$$\tilde{G}_{z\phi}^{E_n} = \frac{nk_z}{\varepsilon_j \rho'} f_{11} - j\omega \frac{\partial f_{12}}{\partial \rho'} \tag{A7}$$

$$\tilde{G}_{z\phi}^{H_n} = \frac{nk_z}{\varepsilon_j \rho'} f_{21} - j\omega \frac{\partial f_{22}}{\partial \rho'} \tag{A8}$$

$$\tilde{G}_{\phi\phi}^{E_n} = \frac{nk_z}{\varepsilon_j \rho'} \left(\frac{nk_z}{k_{\rho_i}^2 \rho} f_{11} + \frac{j\omega\mu_i}{k_{\rho_i}^2} \frac{\partial f_{21}}{\partial \rho} \right) - j\omega \frac{\partial}{\partial \rho'} \left(\frac{nk_z}{k_{\rho_i}^2 \rho} f_{12} + \frac{j\omega\mu_i}{k_{\rho_i}^2} \frac{\partial f_{22}}{\partial \rho} \right) \tag{A9}$$

$$\tilde{G}_{\phi\phi}^{H_n} = \frac{nk_z}{\varepsilon_j \rho'} \left(-\frac{j\omega\varepsilon_i}{k_{\rho_i}^2} \frac{\partial f_{11}}{\partial \rho} + \frac{nk_z}{k_{\rho_i}^2 \rho} f_{21} \right) - j\omega \frac{\partial}{\partial \rho'} \left(-\frac{j\omega\varepsilon_i}{k_{\rho_i}^2} \frac{\partial f_{12}}{\partial \rho} + \frac{nk_z}{k_{\rho_i}^2 \rho} f_{22} \right) \tag{A10}$$

$$\tilde{G}^{E_n}_{\rho\phi} = \frac{nk_z}{\varepsilon_j\rho'}\left(-\frac{jk_z}{k^2_{\rho_i}}\frac{\partial f_{11}}{\partial\rho}+\frac{\omega\mu_i n}{k^2_{\rho_i}\rho}f_{21}\right)-j\omega\frac{\partial}{\partial\rho'}\left(-\frac{jk_z}{k^2_{\rho_i}}\frac{\partial f_{12}}{\partial\rho}+\frac{\omega\mu_i n}{k^2_{\rho_i}\rho}f_{22}\right) \tag{A11}$$

$$\tilde{G}^{H_n}_{\rho\phi} = \frac{nk_z}{\varepsilon_j\rho'}\left(-\frac{\omega\varepsilon_i n}{k^2_{\rho_i}\rho}f_{11}-\frac{jk_z}{k^2_{\rho_i}}\frac{\partial f_{21}}{\partial\rho}\right)-j\omega\frac{\partial}{\partial\rho'}\left(-\frac{\omega\varepsilon_i n}{k^2_{\rho_i}\rho}f_{12}-\frac{jk_z}{k^2_{\rho_i}}\frac{\partial f_{22}}{\partial\rho}\right) \tag{A12}$$

ρ-oriented electric dipole:

$$\tilde{G}^{E_n}_{z\rho} = \left(\frac{jk_z}{\varepsilon_j}\frac{\partial f_{11}}{\partial\rho'}+\frac{n\omega}{\rho'}f_{12}\right) \tag{A13}$$

$$\tilde{G}^{E_n}_{\phi\rho} = \frac{1}{k^2_{\rho_i}}\left(\frac{k_z n}{\rho}\left(\frac{jk_z}{\varepsilon_j}\frac{\partial f_{11}}{\partial\rho'}+\frac{n\omega}{\rho'}f_{12}\right)+j\omega\mu_i\frac{\partial}{\partial\rho}\left(\frac{jk_z}{\varepsilon_j}\frac{\partial f_{21}}{\partial\rho'}+\frac{n\omega}{\rho'}f_{22}\right)\right) \tag{A14}$$

$$\tilde{G}^{E_n}_{\rho\rho} = \frac{1}{k^2_{\rho_i}}\left(-jk_z\frac{\partial}{\partial\rho}\left(\frac{jk_z}{\varepsilon_j}\frac{\partial f_{11}}{\partial\rho'}+\frac{n\omega}{\rho'}f_{12}\right)+\frac{\omega n\mu_i}{\rho}\left(\frac{jk_z}{\varepsilon_j}\frac{\partial f_{21}}{\partial\rho'}+\frac{n\omega}{\rho'}f_{22}\right)\right) \tag{A15}$$

$$\tilde{G}^{H_n}_{z\rho} = \frac{jk_z}{\varepsilon_j}\frac{\partial f_{21}}{\partial\rho'}+\frac{n\omega}{\rho'}f_{22} \tag{A16}$$

$$\tilde{G}^{H_n}_{\phi\rho} = \frac{1}{k^2_{\rho_i}}\left[-j\omega\varepsilon_i\frac{\partial}{\partial\rho}\left(\frac{jk_z}{\varepsilon_j}\frac{\partial f_{11}}{\partial\rho'}+\frac{n\omega}{\rho'}f_{12}\right)+\frac{k_z n}{\rho}\left(\frac{jk_z}{\varepsilon_j}\frac{\partial f_{21}}{\partial\rho'}+\frac{n\omega}{\rho'}f_{22}\right)\right] \tag{A17}$$

$$\tilde{G}^{H_n}_{\rho\rho} = \frac{1}{k^2_{\rho_i}}\left(-\frac{n\omega\varepsilon_i}{\rho}\left(\frac{jk_z}{\varepsilon_j}\frac{\partial f_{11}}{\partial\rho'}+\frac{n\omega}{\rho'}f_{12}\right)-jk_z\frac{\partial}{\partial\rho}\left(\frac{jk_z}{\varepsilon_j}\frac{\partial f_{21}}{\partial\rho'}+\frac{n\omega}{\rho'}f_{22}\right)\right) \tag{A18}$$

z-oriented magnetic dipole:

$$\tilde{G}^{E_n}_{zz} = \frac{k^2_{\rho_j}}{\mu_j}f_{12} \tag{A19}$$

$$\tilde{G}^{H_n}_{zz} = \frac{k^2_{\rho_j}}{\mu_j}f_{22} \tag{A20}$$

$$\tilde{G}^{E_n}_{\phi z} = \frac{k^2_{\rho_j}}{\mu_j}\left(\frac{nk_z}{k^2_{\rho_j}\rho}f_{12}+\frac{j\omega\mu_i}{k^2_{\rho_j}}\frac{\partial f_{22}}{\partial\rho}\right) \tag{A21}$$

$$\tilde{G}^{H_n}_{\phi z} = \frac{k^2_{\rho_j}}{\mu_j}\left(-\frac{j\omega\varepsilon_i}{k^2_{\rho_i}}\frac{\partial f_{12}}{\partial\rho}+\frac{nk_z}{k^2_{\rho_i}\rho}f_{22}\right) \tag{A22}$$

$$\tilde{G}^{E_n}_{\rho z} = \frac{k^2_{\rho_j}}{\mu_j}\left(-\frac{jk_z}{k^2_{\rho_i}}\frac{\partial f_{12}}{\partial \rho} + \frac{\omega\mu_i n}{\rho k^2_{\rho_i}} f_{22}\right) \tag{A23}$$

$$\tilde{G}^{H_n}_{\rho z} = \frac{k^2_{\rho_j}}{\mu_j}\left(\frac{-\omega\varepsilon_i n}{k^2_{\rho_i}\rho} f_{12} - \frac{jk_z}{k^2_{\rho_i}}\frac{\partial f_{22}}{\partial \rho}\right) \tag{A24}$$

ϕ-oriented magnetic dipole:

$$\tilde{G}^{E_n}_{z\phi} = j\omega\frac{\partial f_{11}}{\partial \rho'} + \frac{nk_z}{\mu_j \rho'} f_{12} \tag{A25}$$

$$\tilde{G}^{H_n}_{z\phi} = j\omega\frac{\partial f_{21}}{\partial \rho'} + \frac{nk_z}{\mu_j \rho'} f_{22} \tag{A26}$$

$$\tilde{G}^{E_n}_{\phi\phi} = j\omega\frac{\partial}{\partial \rho'}\left(\frac{nk_z}{k^2_{\rho_i}\rho} f_{11} + \frac{j\omega\mu_i}{k^2_{\rho_i}}\frac{\partial f_{21}}{\partial \rho}\right) + \frac{nk_z}{\mu_j \rho'}\left(\frac{nk_z}{k^2_{\rho_i}\rho} f_{12} + \frac{j\omega\mu_i}{k^2_{\rho_i}}\frac{\partial f_{22}}{\partial \rho}\right) \tag{A27}$$

$$\tilde{G}^{H_n}_{\phi\phi} = j\omega\frac{\partial}{\partial \rho'}\left(-\frac{j\omega\varepsilon_i}{k^2_{\rho_i}}\frac{\partial f_{11}}{\partial \rho} + \frac{nk_z}{k^2_{\rho_i}\rho} f_{21}\right) + \frac{nk_z}{\mu_j \rho'}\left(-\frac{j\omega\varepsilon_i}{k^2_{\rho_i}}\frac{\partial f_{12}}{\partial \rho} + \frac{nk_z}{k^2_{\rho_i}\rho} f_{22}\right) \tag{A28}$$

$$\tilde{G}^{E_n}_{\rho\phi} = j\omega\frac{\partial}{\partial \rho'}\left(-\frac{jk_z}{k^2_{\rho_i}}\frac{\partial f_{11}}{\partial \rho} + \frac{\omega\mu_i n}{k^2_{\rho_i}\rho} f_{21}\right) + \frac{nk_z}{\mu_j \rho'}\left(-\frac{jk_z}{k^2_{\rho_i}}\frac{\partial f_{12}}{\partial \rho} + \frac{\omega\mu_i n}{k^2_{\rho_i}\rho} f_{22}\right) \tag{A29}$$

$$\tilde{G}^{H_n}_{\rho\phi} = j\omega\frac{\partial}{\partial \rho'}\left(\frac{-\omega\varepsilon_i n}{k^2_{\rho_i}\rho} f_{11} - \frac{jk_z}{k^2_{\rho_i}}\frac{\partial f_{21}}{\partial \rho}\right) + \frac{nk_z}{\mu_j \rho'}\left(-\frac{\omega\varepsilon_i n}{k^2_{\rho_i}\rho} f_{12} - \frac{jk_z}{k^2_{\rho_i}}\frac{\partial f_{22}}{\partial \rho}\right) \tag{A30}$$

ρ-oriented magnetic dipole:

$$\tilde{G}^{E_n}_{z\rho} = \left(-\frac{n\omega}{\rho'} f_{11} + \frac{jk_z}{\mu_j}\frac{\partial f_{12}}{\partial \rho'}\right) \tag{A31}$$

$$\tilde{G}^{E_n}_{\phi\rho} = \frac{1}{k^2_{\rho_i}}\left(\frac{k_z n}{\rho}\left(-\frac{n\omega}{\rho'} f_{11} + \frac{jk_z}{\mu_j}\frac{\partial f_{12}}{\partial \rho'}\right) + j\omega\mu_i\frac{\partial}{\partial \rho}\left(-\frac{n\omega}{\rho'} f_{21} + \frac{jk_z}{\mu_j}\frac{\partial f_{22}}{\partial \rho'}\right)\right) \tag{A32}$$

$$\tilde{G}^{E_n}_{\rho\rho} = \frac{1}{k^2_{\rho_i}}\left(-jk_z\frac{\partial}{\partial \rho}\left(-\frac{n\omega}{\rho'} f_{11} + \frac{jk_z}{\mu_j}\frac{\partial f_{12}}{\partial \rho'}\right) + \frac{\omega\mu_i n}{\rho}\left(-\frac{n\omega}{\rho'} f_{21} + \frac{jk_z}{\mu_j}\frac{\partial f_{22}}{\partial \rho'}\right)\right) \tag{A33}$$

$$\tilde{G}_{z\rho}^{H_n} = \left(-\frac{n\omega}{\rho'} f_{21} + \frac{jk_z}{\mu_j}\frac{\partial f_{22}}{\partial \rho'}\right) \tag{A34}$$

$$\tilde{G}_{\phi\rho}^{H_n} = \frac{1}{k_{\rho_i}^2}\left(-j\omega\varepsilon_i\frac{\partial}{\partial\rho}\left(-\frac{n\omega}{\rho'} f_{11} + \frac{jk_z}{\mu_j}\frac{\partial f_{12}}{\partial\rho'}\right) + \frac{k_z n}{\rho}\left(-\frac{n\omega}{\rho'} f_{21} + \frac{jk_z}{\mu_j}\frac{\partial f_{22}}{\partial\rho'}\right)\right) \tag{A35}$$

$$\tilde{G}_{\rho\rho}^{H_n} = \frac{1}{k_{\rho_i}^2}\left(-\frac{n\omega\varepsilon_i}{\rho}\left(-\frac{n\omega}{\rho'} f_{11} + \frac{jk_z}{\mu_j}\frac{\partial f_{12}}{\partial\rho'}\right) - jk_z\frac{\partial}{\partial\rho}\left(-\frac{n\omega}{\rho'} f_{21} + \frac{jk_z}{\mu_j}\frac{\partial f_{22}}{\partial\rho'}\right)\right) \tag{A36}$$

with

$$\overline{F}_n(\rho,\rho') = \begin{bmatrix} f_{11} & f_{12} \\ f_{21} & f_{22} \end{bmatrix} = \begin{cases} \left[J_n(k_{\rho_i}\rho)\overline{I} + H_n^2(k_{\rho_i}\rho)\tilde{\overline{R}}_{i,i-1}\right] \\ \cdot\tilde{\overline{T}}_{j,i}\cdot\tilde{\overline{M}}_{j-}\cdot\left[H_n^2(k_{\rho_j}\rho')\overline{I} + J_n(k_{\rho_j}\rho')\tilde{\overline{R}}_{j,j+1}\right], \ i<j \\ \left[H_n^2(k_{\rho_i}\rho)\overline{I} + J_n(k_{\rho_i}\rho)\tilde{\overline{R}}_{i,i+1}\right] \\ \cdot\tilde{\overline{T}}_{j,i}\cdot\tilde{\overline{M}}_{j+}\cdot\left[J_n(k_{\rho_j}\rho')\overline{I} + H_n^2(k_{\rho_j}\rho')\tilde{\overline{R}}_{j,j-1}\right], \ i>j \end{cases}$$

where source and observation points are located in regions j and i, respectively, $\tilde{\overline{R}}_{j,j\mp1}$ is the generalized reflection matrix, $\tilde{\overline{T}}_{i,i\pm1}$ is the generalized transmission matrix and $\tilde{\overline{M}}_{j\mp} = (\overline{I} - \tilde{\overline{R}}_{j,j\pm1}, \tilde{\overline{R}}_{j,j\mp1})^{-1}$ is a factor accounting for multiple reflections in the source region j [21].

Electric or magnetic spectral domain Green's function in α direction due to β-oriented source, $\tilde{G}_{\alpha\beta}^{E,H}$ [21],

$$\tilde{G}_{\alpha\beta}^{E,H} = -\frac{1}{4\omega}\sum_{n=-\infty}^{\infty} e^{jn(\phi-\phi')}\tilde{G}_{\alpha\beta}^{E_n,H_n} = -\frac{1}{4\omega}\sum_{n=-\infty}^{\infty} e^{jn(\phi-\phi')}\overline{F}_n(\rho,\rho')\overleftarrow{S}_n$$

$\overleftarrow{S}_n$ is a 2×1 matrix operator of the form

$$\overleftarrow{S}_n = \begin{bmatrix} \frac{1}{\varepsilon_j}\left(k_j^2\hat{a}_z + jk_z\vec{\nabla}'\right)\cdot\hat{\beta} \\ -jw\hat{\beta}\cdot\left(\hat{a}_z\times\vec{\nabla}'\right) \end{bmatrix}$$

for the fields due to an electric source and

$$\overleftarrow{S}_n = \begin{bmatrix} jw\hat{\beta}\cdot\left(\hat{a}_z\times\vec{\nabla}'\right) \\ \frac{1}{\mu_j}\left(k_j^2\hat{a}_z + jk_z\vec{\nabla}'\right)\cdot\hat{\beta} \end{bmatrix}$$

for the fields due to a magnetic source and $\vec{\nabla}'$ is defined as

$$\vec{\nabla}' = \hat{a}_\rho \frac{\partial}{\partial \rho'} + \hat{a}_\phi \frac{\partial}{\rho' \partial \phi'} + \hat{a}_z \frac{\partial}{\partial z'}$$

REFERENCES

1. Bussey, H. E. and J. H. Richmond, "Scattering by a lossy dielectric circular cylindrical multilayer, numerical values," *IEEE Trans. Antennas Propagat.*, Vol. AP-23, 723–725, Sept. 1975.
2. Alexopoulos, N. G. and A. Nakatani, "Cylindrical substrate microstrip line characterization," *IEEE Trans. Microwave Theory Tech.*, Vol. MTT-35, 843–849, Sept. 1987.
3. Krowne, C. M., "Cylindrical-rectangular microstrip antenna," *IEEE Trans. Antennas Propagat.*, Vol. AP-31, 194–199, Jan. 1983.
4. Ashkenazy, J., S. Shtrikman, and D. Treves, "Electric surface current model for the analysis of microstrip antennas on cylindrical bodies," *IEEE Trans. Antennas Propagat.*, Vol. AP-33, 295–300, Mar. 1985.
5. Luk, K. M., K. F. Lee, and J. S. Dahele, "Analysis of cylindrical-rectangular patch antenna," *IEEE Trans. Antennas Propagat.*, Vol. AP-37, 143–147, Feb. 1989.
6. Luk, K. M. and K. F. Lee, "Characteristics of the cylindrical-circular patch antenna," *IEEE Trans. Antennas Propagat.*, Vol. AP-38, 1119–1123, July 1990.
7. Tam, W. Y., A. K. Y. Lai, and K. M. Luk, "Cylindrical rectangular microstrip antennas with coplanar parasitic patches," *Proc. Inst. Elect. Eng.*, Vol. 142, 300–306, Aug. 1995.
8. Ali, S. M., T. M. Habashy, J. F. Kiang, and J. A. Kong, "Resonance in cylindrical-rectangular and wraparound microstrip structures," *IEEE Trans. Microwave Theory Tech.*, Vol. MTT-37, 1773–1783, Nov. 1989.
9. Habashy, T. M., S. M. Ali, and J. A. Kong, "Input impedance and radiation pattern of cylindrical rectangular and wraparound microstrip antennas," *IEEE Trans. Antennas Propagat.*, Vol. AP-38, 722–731, May 1990.
10. Fonseca, S. B. A. and A. J. Giarola, "Analysis of microstrip wraparound antennas using dyadic Green's functions," *IEEE Trans. Antennas Propagat.*, Vol. AP-31, 248–253, Mar. 1983.
11. Silva, F. C., S. B. A. Fonseca, A. J. M. Soares, and A. J. Giarola, "Analysis of microstrip antennas on circular-cylindrical substrates

with a dielectric overlay," *IEEE Trans. Antennas Propagat.*, Vol. AP-39, 1398–1404, Sept. 1991.

12. Liano, S.-L. and R. J. Vernon, "On the image approximation for electromagnetic wave propagation and PEC scattering in cylindrical harmonics," *Progress In Electromagnetics Research*, PIER 66, 65–88, 2006.
13. Angiulli, G., G. Amendola, and G. D. Massa, "Radiation from dielectric coated elliptic conducting cylinder by assigned electric current distribution," *Progress In Electromagnetics Research*, PIER 57, 131–150, 2006.
14. Shooshtari, A. and A. R. Sebak, "Electromagnetic scattering by parallel metamaterial cylinders," *Progress In Electromagnetics Research*, PIER 57, 165–177, 2006.
15. Hill, S. C. and J. M. Jarem, "Scattering of multilayer concentric elliptical cylinders excited by single mode source," *Progress In Electromagnetics Research*, PIER 55, 209–226, 2005.
16. Toyama, H. and K. Yasumoto, "Electromagnetic scattering from periodic arrays of composite circular cylinder with internal cylindrical scatterers," *Progress In Electromagnetics Research*, PIER 52, 321–323, 2005.
17. Hamid, A.-K., "Axially slotted antenna on a circular or elliptic cylinder coated with metamaterials," *Progress In Electromagnetics Research*, PIER 51, 329–341, 2005.
18. Hamid, A.-K., "Multi-dielectric loaded axially slotted antenna on circular or elliptic cylinder," *Journal of Electromagnetic Waves and Applications*, Vol. 20, No. 9, 1259–1271, 2006.
19. Najjar-Khatirkolaei, B., M. Al-Kanhal, and A. R. Sebak, "Electromagnetic wave scattering by elliptic chiral cylinder," *Journal of Electromagnetic Waves and Applications*, Vol. 20, No. 10, 1377–1390, 2006.
20. Ruppin, R., "Scattering of electromagnetic radiation by perfect electromagnetic conductor cylinder," *Journal of Electromagnetic Waves and Applications*, Vol. 20, No. 13, 1853–1860, 2006.
21. Tokgöz, Ç. and G. Dural, "Closed-form Green's functions for cylindrically stratified media," *IEEE Trans. Microwave Theory and Techniques*, Vol. MTT-48, 40–49, January 2000.
22. Sun, J., C.-F. Wang, L.-W. Li, and M.-S. Leong, "Further improvement for fast computation of mixed potential Green's functions for cylindrically stratified media," *IEEE Trans. Antennas Propagat.*, Vol. AP-52, 3026–3036, Nov. 2004.

23. Acar, R. C., "Numerically efficient analysis and design of conformal printed structures in cylindrically layered media," Ph.D. Thesis, Dept. Elec. Electron. Eng., Middle East Technical Univ., Ankara, Turkey, September 2007.
24. Hua, Y. and T. K. Sarkar, "Generalized pencil-of-function method for extracting poles of an EM system from its transient response," *IEEE Trans. Antennas Propagat.*, Vol. AP-37, 229–234, Feb. 1989.
25. Demirdağ, C. and R. G. Rojas, "Mutual coupling calculations on a dielectric coated PEC cylinder using a UTD-based Green's function," *IEEE Antennas and Propagation Society International Symposium*, Vol. 3, 1525–1528, 1997.
26. Ertürk, V. B. and R. G. Rojas, "Efficient analysis of input impedance and mutual coupling of microstrip antennas mounted on large coated cylinders," *IEEE Trans. Antennas Propagat.*, Vol. AP-51, 739–749, April 2003.
27. Ertürk, V. B., "Efficient hybrid MoM/Green's function technique to analyze conformal microstrip antennas and arrays," Ph.D dissertation, Dept. of Electrical Engineering, Ohio-State University, 2000.
28. Acar, R. C. and G. Dural, "Comments on 'A complete set of spatial domain dyadic Green's function components for cylindrically stratified media in fast computational form'," *Journal of Electromagnetic Waves and Applications*, Vol. 18, No. 10, 1389–1394, 2004.
29. Nakatani A., N. G. Alexopoulos, N. K. Uzunoglu, and P. L. E. Uslenghi, "Accurate Green's function computation for printed circuit antennas on cylindrical substrates," *Electromagnetics*, Vol. 6, 243–254, 1986.